Symmetric Set of Transport Coefficients for Collisional Magnetized Plasma

James D. Sadler,[1,2] Christopher A. Walsh,[3] and Hui Li[1]
[1]Theoretical Division, Los Alamos National Laboratory, Los Alamos, New Mexico 87545, USA
[2]Center for Nonlinear Studies, Los Alamos National Laboratory, Los Alamos, New Mexico 87545, USA
[3]Lawrence Livermore National Laboratory, Livermore, California 94550, USA

(Received 9 September 2020; revised 14 December 2020; accepted 15 January 2021; published 15 February 2021)

Braginskii extended magnetohydrodynamics is used to model transport in collisional astrophysical and high energy density plasmas. We show that commonly used approximations to the $\alpha_\perp$ and $\beta_\perp$ transport coefficients [e.g., Epperlein and Haines, Phys. Fluids **29**, 1029 (1986)] have a subtle inaccuracy that causes significant artificial magnetic dissipation and discontinuities. This is because magnetic transport actually relies on $\beta_\parallel - \beta_\perp$ and $\alpha_\perp - \alpha_\parallel$, rather than $\alpha_\perp$ and $\beta_\perp$ themselves. We provide fit functions that rectify this problem and thus resolve the discrepancies with kinetic simulations in the literature. When implemented in the Gorgon code, they reduce the predicted density asymmetry amplitude at laser ablation fronts. Recognizing the importance of $\alpha_\perp - \alpha_\parallel$ and $\beta_\parallel - \beta_\perp$, we recast the set of coefficients. This makes explicit the symmetry of the magnetic and thermal transport, as well as the symmetry of the coefficients themselves.

DOI: 10.1103/PhysRevLett.126.075001

Treatment of collisional magnetized plasma with the electron-ion two-fluid approach leads to the extended magnetohydrodynamic (ExMHD) theory of plasma transport [1]. This has successfully described magnetic field dynamics in high energy density (HED) plasmas such as Z pinches [2], laser plasmas [3,4], fast ignition fusion concepts [5], dense fusion fuel hot spots [6], and laser ablation fronts [7]. ExMHD results in an intricate set of plasma feedback interactions. Coulomb collisions give rise to Ohmic resistance. Electron temperature gradients produce thermoelectric forces, since hotter electrons are less susceptible to collisions. The resulting magnetic field advection can greatly exceed that due to the ideal advection with the fluid [8]. The magnetic field also insulates and deflects the electron heat flow [4], causing changes to heat confinement and hydrodynamics. Coupling of these effects can result in growth of magnetic fields at the expense of fluid energy [9], under processes such as the thermomagnetic instability [10,11]. ExMHD effects are also important for magnetic reconnection [12] in the weakly collisional plasma found in galaxy clusters and jets. Laboratory experiments emulating these magnetized jets [13] and the turbulent dynamo process [14] also require ExMHD modeling.

Derivation from the kinetic equation [1] showed that the heat flux, resistive, and thermoelectric processes should be described by tensors dependent on the magnetic field $\mathbf{B}$. Typically, simulation codes use an implementation given in Ref. [15], in which the electric field $\mathbf{E}$ was numerically calculated from kinetic theory and then fitted with tabulated functions for the resistive ($\alpha_\parallel$, $\alpha_\perp$, $\alpha_\wedge$) and thermoelectric ($\beta_\parallel$, $\beta_\perp$, $\beta_\wedge$) transport coefficients. Studies using the ExMHD codes Gorgon [6] and Hydra [16] found that heat insulation from self-generated magnetic fields can significantly change HED plasma temperature profiles. Accurate transport coefficients are therefore of considerable importance.

In this work, we show that, rather than $\alpha_\perp$ and $\beta_\perp$, the primary quantities for magnetic transport are $\alpha_\perp - \alpha_\parallel$ and $\beta_\parallel - \beta_\perp$. Recasting the coefficient set in terms of these quantities reveals the inherent symmetry between the magnetic and heat transport, and the symmetry of the coefficients themselves. This was not recognized in the fit functions of Ref. [15], leading to inaccurate values when calculating $\alpha_\perp - \alpha_\parallel$ and $\beta_\parallel - \beta_\perp$. This means that many ExMHD simulations in the literature, for example those using the Gorgon [6,7], Hydra [16,17], and CTC [18] codes, have suffered fundamentally incorrect magnetic transport, resulting in discontinuities. We provide new fit functions that correctly reproduce the behavior of detailed kinetic calculations, and then implement them in the Gorgon code. Comparisons show that previous ExMHD simulations have significantly overestimated the cross-gradient Nernst advection and the resulting magnetic dissipation. This then invalidates the magnetized thermal transport and hydrodynamics. For example, the new fits reduce the predicted asymmetry of inertial confinement fusion laser ablation fronts.

The magnetic transport is described by the tensor ExMHD generalized Ohm's law, given by [1,15]

$$\mathbf{E} = -\mathbf{u}\times\mathbf{B} + \frac{\mathbf{J}\times\mathbf{B}}{n_e e} - \frac{\nabla\cdot\underline{P}_e}{n_e e} + \frac{m_e\underline{\alpha}\cdot\mathbf{J}}{n_e e^2\tau} - \frac{\underline{\beta}\cdot\nabla T_e}{e}, \quad (1)$$

$$\underline{\alpha}\cdot\mathbf{J}=\alpha_{\parallel}(\mathbf{J}\cdot\hat{\mathbf{b}})\hat{\mathbf{b}}+\hat{\mathbf{b}}\times(\alpha_{\perp}\mathbf{J}\times\hat{\mathbf{b}}-\alpha_{\wedge}\mathbf{J}), \quad (2)$$

$$\underline{\beta}\cdot\nabla T_e=\beta_{\parallel}(\nabla T_e\cdot\hat{\mathbf{b}})\hat{\mathbf{b}}+\hat{\mathbf{b}}\times(\beta_{\perp}\nabla T_e\times\hat{\mathbf{b}}+\beta_{\wedge}\nabla T_e). \quad (3)$$

The first term in Eq. (1) is the relativistic transformation from the ion fluid rest frame at velocity $\mathbf{u}$ and, taken alone, yields ideal MHD. The Ohm's law also depends on the electron charge $-e$, mass m_e, number density n_e, and temperature T_e. In quasineutral plasma $n_e=\sum_j n_j Z_j$, where n_j is the number density of ion species j with ionization Z_j. Electric fields also arise due to currents $\mathbf{J}$, and due to gradients in the electron pressure tensor $\underline{P}_e$. The inertial term has been neglected.

Coulomb collisions cause the final two terms in Eq. (1). They are decomposed into an orthogonal basis parallel and perpendicular to the field direction $\hat{\mathbf{b}}=\mathbf{B}/|\mathbf{B}|$. Each component has its own dimensionless and positive transport coefficient $\alpha_{\perp}(\chi,\bar{Z})$, $\alpha_{\wedge}(\chi,\bar{Z})$, and $\alpha_{\parallel}(\bar{Z})=\alpha_{\perp}(0,\bar{Z})$. Together these describe the magnetized deflection and inhibition of currents. Similarly, the collisional thermal force or thermoelectric term in Eq. (3) is driven by electron temperature gradients and depends on the coefficients $\beta_{\perp}(\chi,\bar{Z})$, $\beta_{\wedge}(\chi,\bar{Z})$, and $\beta_{\parallel}(\bar{Z})=\beta_{\perp}(0,\bar{Z})$. These are functions of the average ion charge state $\bar{Z}=(\sum_j n_j Z_j^2)/(\sum_j n_j Z_j)$ and the dimensionless electron magnetization

$$\chi=\frac{e|\mathbf{B}|\tau}{m_e}\simeq\frac{6\times10^{16}}{\bar{Z}\ln(\Lambda)}\left(\frac{T_e}{\mathrm{eV}}\right)^{\frac{3}{2}}\left(\frac{n_e}{\mathrm{cm}^{-3}}\right)^{-1}\left(\frac{|\mathbf{B}|}{\mathrm{T}}\right), \quad (4)$$

where the electron Coulomb collision time is

$$\tau=\frac{3\sqrt{\pi}}{4}\frac{4\pi\epsilon_0^2 m_e^2 v_{\mathrm{th}}^3}{n_e\bar{Z}e^4\ln(\Lambda)}. \quad (5)$$

These expressions contain the electron-ion Coulomb logarithm [assumed to be $\ln(\Lambda)\gg1$], the vacuum permittivity ϵ_0 and the electron thermal speed $v_{\mathrm{th}}=\sqrt{2T_e/m_e}$.

We now make the standard MHD assumption to retain only slow oscillations and therefore neglect displacement current, yielding $\mathbf{J}=c^2\epsilon_0\nabla\times\mathbf{B}$. Following Ref. [19], manipulation of Eqs. (1)–(3), using the vector components $\mathbf{J}=\hat{\mathbf{b}}(\mathbf{J}\cdot\hat{\mathbf{b}})+\hat{\mathbf{b}}\times(\mathbf{J}\times\hat{\mathbf{b}})$, leads to the simplified form

$$\mathbf{E}=-\mathbf{u}_B\times\mathbf{B}+D_{\parallel}\nabla\times\mathbf{B}-\frac{\nabla\cdot\underline{P}_e}{n_e e}-\frac{\beta_{\parallel}}{e}\nabla T_e, \quad (6)$$

$$\mathbf{u}_B=\mathbf{u}-(1+\delta_{\perp})\frac{\mathbf{J}}{n_e e}+\delta_{\wedge}\frac{\mathbf{J}\times\hat{\mathbf{b}}}{n_e e}-\gamma_{\perp}\frac{\tau}{m_e}\nabla T_e+\gamma_{\wedge}\frac{\tau}{m_e}\nabla T_e\times\hat{\mathbf{b}}, \quad (7)$$

where we have defined the magnetic advection velocity $\mathbf{u}_B$ and the resistive magnetic diffusivity $D_{\parallel}=m_e c^2\epsilon_0\alpha_{\parallel}/(n_e e^2\tau)$. The required α and β combinations motivate the definition of new transport coefficients [19]

$$\delta_{\perp}(\chi,\bar{Z})=\frac{\alpha_{\wedge}}{\chi}, \qquad \gamma_{\perp}(\chi,\bar{Z})=\frac{\beta_{\wedge}}{\chi}, \quad (8)$$

$$\delta_{\wedge}(\chi,\bar{Z})=\frac{\alpha_{\perp}-\alpha_{\parallel}}{\chi}, \qquad \gamma_{\wedge}(\chi,\bar{Z})=\frac{\beta_{\parallel}-\beta_{\perp}}{\chi}. \quad (9)$$

The evolution of $\mathbf{B}$ is then found via Faraday's law $\partial_t\mathbf{B}=-\nabla\times\mathbf{E}$. In order of appearance, the terms in Eq. (6) are then responsible for advection of $\mathbf{B}$ with velocity $\mathbf{u}_B$, resistive diffusion of $\mathbf{B}$, the Biermann battery source term, and the Z-gradient source term [20,21]. This form of Ohm's law has the advantage that the sole appearance of ExMHD effects, that is, the $\perp$ and $\wedge$ coefficients, is within the magnetic advection velocity $\mathbf{u}_B$ in Eq. (7). The coefficients $D_{\parallel}$ and $\beta_{\parallel}$ for the other terms in Eq. (6) are those from the simpler resistive-MHD model and they do not depend on $\mathbf{B}$.

In addition to the usual $D_{\parallel}$ resistive diffusion, the $\delta_{\perp}$ and $\delta_{\wedge}$ resistive terms alter the Hall velocity $-\mathbf{J}/(n_e e)$ in Eq. (7), both in the parallel and transverse directions. Similarly, the thermal force causes Nernst advection [22,23] of $\mathbf{B}$ down the temperature gradient and cross-gradient Nernst advection perpendicular to it, with coefficients $\gamma_{\perp}$ and $\gamma_{\wedge}$, respectively [16,19,24–26].

We note that it is not the $\alpha_{\parallel}$, $\alpha_{\perp}$, $\beta_{\parallel}$, and $\beta_{\perp}$ coefficients that dictate magnetic transport, but rather the differences between them. This is recognized in the definitions in Eq. (9). However, we later show that the fits from Ref. [15] cannot accurately calculate $\delta_{\wedge}$ and $\gamma_{\wedge}$.

The δ and γ coefficients are fundamental in exposing the symmetry of the magnetic and thermal transport. This becomes apparent when Eq. (7) is compared with the electron heat flow [15]

$$\mathbf{q}_e=-\frac{n_e T_e\tau}{m_e}\underline{\kappa}\cdot\nabla T_e-\frac{T_e}{e}\underline{\beta}\cdot\mathbf{J}. \quad (10)$$

The total electron energy flux, including the enthalpy flux and heat flow, is given by $U_e\mathbf{u}_e+\underline{P}_e\cdot\mathbf{u}_e+\mathbf{q}_e$, where $U_e=m_e n_e|\mathbf{u}_e|^2/2+\mathrm{Tr}(\underline{P}_e)/2$ is the electron fluid energy density and $\mathbf{u}_e=\mathbf{u}-\mathbf{J}/(n_e e)$. Taking isotropic electron pressure with $\underline{P}_e=n_e T_e\underline{I}$ and assuming $|\mathbf{u}_e|\ll v_{\mathrm{th}}$, this total energy flux can be written as $n_e T_e\mathbf{u}_{\mathbf{q}}$, with

$$\mathbf{u}_{\mathbf{q}}=\frac{5}{2}\mathbf{u}-\left(\frac{5}{2}+\beta_{\perp}\right)\frac{\mathbf{J}}{n_e e}+\beta_{\wedge}\frac{\mathbf{J}\times\hat{\mathbf{b}}}{n_e e}-\kappa_{\perp}\frac{\tau}{m_e}\nabla T_e+\kappa_{\wedge}\frac{\tau}{m_e}\nabla T_e\times\hat{\mathbf{b}}-(\beta_{\parallel}-\beta_{\perp})\frac{(\mathbf{J}\cdot\hat{\mathbf{b}})}{n_e e}\hat{\mathbf{b}}-(\kappa_{\parallel}-\kappa_{\perp})\frac{\tau}{m_e}(\hat{\mathbf{b}}\cdot\nabla T_e)\hat{\mathbf{b}}. \quad (11)$$

After replacing the δ and γ coefficients with their β and κ counterparts, Eqs. (7) and (11) are almost equivalent. The only differences are the greater coefficient of $\mathbf{u}$ and the

additional corrections along $\hat{\mathbf{b}}$ in Eq. (11), whereas magnetic advection along $\mathbf{B}$ is not possible.

It turns out that, by defining the δ and γ coefficients to bring Eqs. (7) and (11) into a symmetric form, the coefficients themselves become symmetric. To show this, we must calculate them using Eqs. (8) and (9). Using the results of Braginskii [1], this results in $\lim_{\chi\to 0}\gamma_\wedge = 0$, such that weak magnetic fields are Nernst advected purely down the temperature gradient. Epperlein and Haines (EH) [15] later improved the coefficient dependencies for $\chi \to \infty$. However, the importance of accurately calculating $\alpha_\perp - \alpha_\parallel$ and $\beta_\parallel - \beta_\perp$ was not recognized in the EH fits, or in other more recent works [27–29]. As a result, the EH approximation for $\beta_\perp$ implies that $\lim_{\chi\to 0}\gamma_\wedge \simeq 1$, resulting in a diagonal total Nernst advection across ∇T_e. Although superficially in agreement with Braginskii, the EH fits therefore produce fundamentally different magnetic transport for $\chi \ll 1$. There is a similar disagreement for $\lim_{\chi\to 0}\delta_\wedge$ and the cross-Hall transport.

We now resolve this discrepancy and provide new fit functions. Our kinetic results follow those of Ref. [15], in which electrons are treated with the Fokker-Planck equation, with static ions. The electron distribution function is expanded [30,31] into its isotropic and anisotropic parts via $f_e(\mathbf{v}) = f_0(v) + \mathbf{v}\cdot\mathbf{f}_1(v)/v$, where $v = |\mathbf{v}|$. This is valid for plasma with shallow gradients, such that $v_{\rm th}\tau|\nabla T_e|/T_e \ll 1$ and $v_{\rm th}\tau|\nabla n_e|/n_e \ll 1$. This local assumption yields a Maxwellian $f_0 \simeq n_e/(v_{\rm th}\sqrt{\pi})^3 \exp(-v^2/v_{\rm th}^2)$. Several authors [32–34] have examined departures from this assumption. In a uniform plasma, $\mathbf{f}_1$ reaches a steady state given by

$$\frac{e}{m_e}\left(\mathbf{E}\frac{df_0}{dv} + \mathbf{B}\times\mathbf{f}_1\right) - \frac{3\sqrt{\pi}}{4}\frac{v_{\rm th}^3}{v^3}\frac{\mathbf{f}_1}{\tau} + \mathbf{C}_{ee} = 0. \quad (12)$$

The electron-ion collision operator in Eq. (12) is a decay of $\mathbf{f}_1$ on a timescale τ, whereas the electron-electron operator $\mathbf{C}_{ee}$ is more complex and is given in Ref. [31].

Equation (12) was solved numerically via an explicit iterative method, using fourth order numerical integrals and finite differences. The uniform velocity grid extended to $8v_{\rm th}$ with resolution $v_{\rm th}/15$. We assumed a fixed electric field and varied the transverse magnetic field. The steady state $\mathbf{f}_1$ was then numerically integrated [30] to yield the current $\mathbf{J} = -(4\pi e/3)\int_0^\infty \mathbf{f}_1 v^3 dv$ and heat flux $\mathbf{q}_e = 5T_e\mathbf{J}/(2e) + (2\pi m_e/3)\int_0^\infty \mathbf{f}_1 v^5 dv$. The α, β, δ, and γ coefficients are then found from Eqs. (1), (2), (10) and (8), (9), using the fact that $\nabla T_e = \mathbf{u} = 0$.

The results for $\delta_\wedge$ and $\gamma_\wedge$ are presented in Fig. 1, alongside estimates using the EH fit functions [15] in Eq. (9). The EH fits are sufficiently accurate to calculate $\delta_\perp$ and $\gamma_\perp$ with Eq. (8), but should not be used to calculate $\delta_\wedge$ and $\gamma_\wedge$ for $\chi < 1$ with Eq. (9). Some new fit functions, remaining simultaneously accurate for $\alpha_\perp$, $\beta_\perp$, $\delta_\wedge$, and $\gamma_\wedge$, are given by

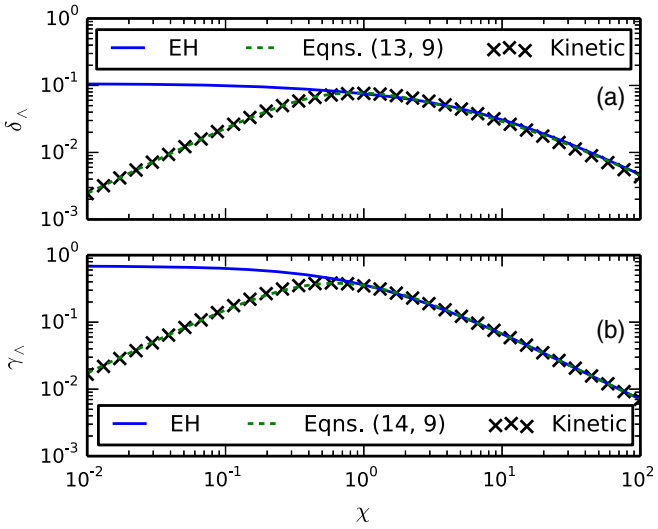

FIG. 1. Plots of the kinetic (a) $\delta_\wedge$ cross-Hall and (b) $\gamma_\wedge$ cross-Nernst transport coefficients for $\bar{Z} = 1$, fitted using Eqs. (13) and (14) in Eq. (9). The results of Epperlein and Haines (EH) [15] are only accurate for $\chi > 1$.

$$\alpha_\perp(\chi,\bar{Z}) = \alpha_\parallel + \frac{\chi^2 + (1-\alpha_\parallel)\chi^3}{\alpha_0 + \alpha_1\chi + \alpha_2\chi^2 + \chi^3}, \quad (13)$$

$$\beta_\perp(\chi,\bar{Z}) = \beta_\parallel \frac{1 + \frac{8}{9}\beta_1\chi}{(1 + \beta_1\chi + \beta_2\chi^2 + \beta_3\chi^3)^{8/9}}. \quad (14)$$

The dashed green curves in Fig. 1 show the result of substituting these fit functions into Eq. (9). The α_j and β_j fit parameters were found using a Powell optimization algorithm and are tabulated for arbitrary $\bar{Z} \geq 1$ in the Supplemental Material [35]. The unphysical aspect of the EH fits is a degree of freedom that allows $(\partial\alpha_\perp/\partial\chi)|_{\chi=0} \neq 0$ and $(\partial\beta_\perp/\partial\chi)|_{\chi=0} \neq 0$. This is removed for Eqs. (13) and (14), which have an enforced zero derivative.

The full set of δ, γ, β, and κ transport coefficients are plotted in Fig. 2 for the case $\bar{Z} = 1$. Together with $\alpha_\parallel(\bar{Z})$ and $\beta_\parallel(\bar{Z})$, these constitute a complete set. It is now obvious why we have labeled these the symmetric coefficients, since, in contrast to the (now defunct) $\alpha_\perp$ coefficient, all of them now have the same overall shape. By defining the δ and γ coefficients to bring Eqs. (7) and (11) into their symmetric form, the set of transport coefficients also becomes symmetric.

To assess the impact of the new fit functions on experimental predictions, they were implemented in the ExMHD code Gorgon [19]. A test problem investigated perturbation smoothing within a direct-drive inertial confinement fusion ablation front. The simulation used a two-dimensional azimuthally symmetric spherical coordinate system with resolution 1 μm in r and 0.25° in θ. The 430 μm outer radius carbon hydrogen (CH) capsule was

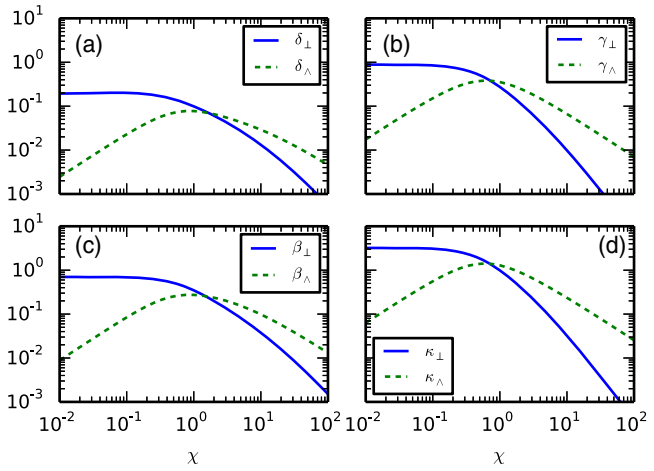

FIG. 2. The symmetric form of the transport coefficients for $\bar{Z} = 1$. (a) The Hall coefficients $\delta_\perp$ and $\delta_\wedge$. (b) The Nernst coefficients $\gamma_\perp$ and $\gamma_\wedge$. (c) The thermoelectric coefficients $\beta_\perp$ and $\beta_\wedge$. (d) The Spitzer coefficients $\kappa_\perp$ and $\kappa_\wedge$.

irradiated with a 1 ns, 18 kJ laser drive, producing intensity 7×10^{14} W cm^{-2}. The laser had a $\pm 10\%$ amplitude mode 12 sinusoidal power perturbation along θ, leading to hydrodynamic imprint and self-generation of azimuthal magnetic field via the Biermann battery. For these conditions, Hall transport is negligible and $\mathbf{u}_B$ is dominated by the ideal and Nernst terms. The simulations used heat flux limiter 0.06 and multigroup radiation transport. The simulations match those detailed in Ref. [26], albeit with no premagnetization.

The results are plotted in Fig. 3. The magnetic field reaches 40T after 1 ns, producing electron gyroradius

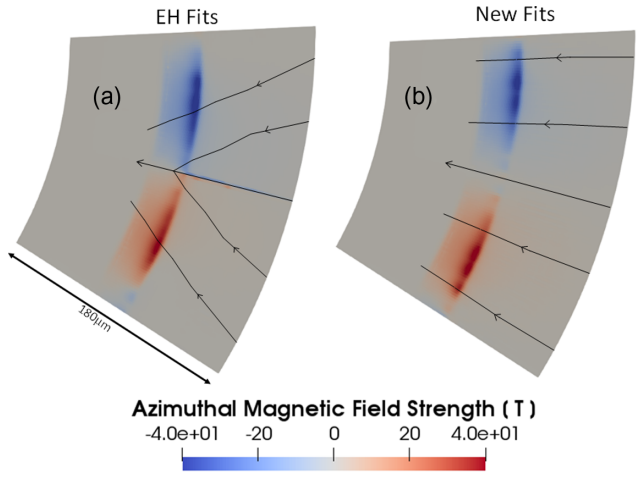

FIG. 3. Magnetic field from the 2D ExMHD Gorgon simulations of a perturbed direct-drive laser ablation front, shown after 1 ns. Simulations used the transport coefficient fits of (a) Epperlein and Haines (EH) [15] and (b) this work. Streamlines show the total Nernst velocity, calculated using the final two terms of Eq. (7).

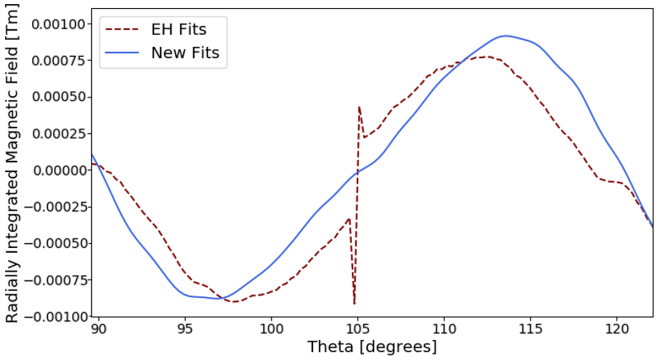

FIG. 4. Comparison of the radially integrated azimuthal **B** field for the two cases, shown after 1 ns.

$\simeq 3$ μm and maximal $\chi \simeq 0.03$. The magnetic field has the same mode 12 profile as the laser perturbation. It is compressed into the conduction zone because the inward Nernst advection exceeds the outward ideal advection.

The EH fit functions [15] predict a finite cross-gradient Nernst velocity $\simeq(\tau/m_e)\nabla T_e \times \hat{\mathbf{b}}$ for these weak fields [Fig. 1(b)], resulting in diagonal total Nernst streamlines in Fig. 3(a). At spatial positions with $|\mathbf{B}| = 0$, $\hat{\mathbf{b}}$ is undefined, yielding a discontinuity. The new fit functions, on the other hand, predict no such discontinuity and give predominantly radial total Nernst advection in Fig. 3(b).

The effect of this transport on the radially integrated magnetic field profile is shown in Fig. 4. The EH fits artificially advect opposite polarity **B** field regions together. This results in a discontinuity and a shift of the field profile. This artificial shift has majorly impacted the magnetized heat conduction profile in ExMHD simulations, and is therefore of more than just theoretical interest. For example, Fig. 5 shows the areal mass density. The updated magnetic transport predicts a reduced density perturbation amplitude when compared to the simulation using the EH fits. Since these perturbations are a seed for implosion fluid instabilities, a major degradation mechanism, this improved magnetic transport could significantly affect the overall fusion performance.

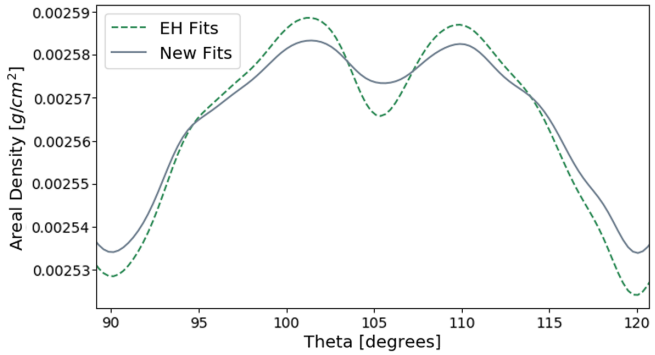

FIG. 5. Comparison of the radially integrated mass density for the two cases, shown after 1 ns.

In fact, there are many other improvements when comparing ExMHD to previous kinetic results. In the 2D simulations of Hill and Kingham [36] with $\chi < 0.1$, the cross-gradient Nernst velocity was 3 orders of magnitude less than the standard Nernst velocity, in agreement with Fig. 3(b). This remained true even in the denser regions close to the target, where classical transport theory is expected to hold. A comparative lack of cross-gradient Nernst advection was also observed in kinetic simulations of the thermomagnetic instability, both with a Vlasov-Fokker-Planck [11] and particle-in-cell [37] approach.

In summary, we have shown that, once recast into a new set, all of the transport coefficients have the same behavior. This elucidates the symmetry of the magnetic and thermal transport in a collisional magnetized plasma. To accurately calculate magnetic transport for $\chi < 1$, the fit functions of Epperlein and Haines [15] must be updated. These previous fit functions massively overestimated the cross-Nernst and cross-Hall advection, causing artificial magnetic discontinuities and dissipation. The new fits also explain the apparent discrepancies between kinetic simulations [36] and ExMHD simulations in the literature. This more natural and accurate description of magnetic transport will improve modeling capabilities for a wide range of magnetized HED plasma experiments.

Research presented in this Letter was supported by Los Alamos National Laboratory under Laboratory Directed Research and Development Project No. 20180040DR and the Center for Nonlinear Studies. This work was performed under the auspices of the U.S. Department of Energy by Lawrence Livermore National Laboratory under Contract No. DE-AC52-07NA27344. This document was prepared as an account of work sponsored by an agency of the United States government. Neither the United States government nor Lawrence Livermore National Security, LLC, nor any of their employees makes any warranty, expressed or implied, or assumes any legal liability or responsibility for the accuracy, completeness, or usefulness of any information disclosed. The views and opinions of the authors expressed herein do not necessarily state or reflect those of the United States government or Lawrence Livermore National Security, LLC, and shall not be used for advertising or product endorsement purposes.

Note added.—During review, the authors were made aware of similar recent work by Davies *et al.* [38].

[1] S. I. Braginskii, Sov. Phys. JETP **6**, 358 (1958).
[2] M. G. Haines, Plasma Phys. Controlled Fusion **53**, 093001 (2011).
[3] M. G. Haines, Can. J. Phys. **64**, 912 (1986).
[4] D. H. Froula, J. S. Ross, B. B. Pollock, P. Davis, A. N. James, L. Divol, M. J. Edwards, A. A. Offenberger, D. Price, R. P. J. Town *et al.*, Phys. Rev. Lett. **98**, 135001 (2007).
[5] P. Nicolaï, J.-L. Feugeas, C. Regan, M. Olazabal-Loumé, J. Breil, B. Dubroca, J.-P. Morreeuw, and V. Tikhonchuk, Phys. Rev. E **84**, 016402 (2011).
[6] C. A. Walsh, J. P. Chittenden, K. McGlinchey, N. P. L. Niasse, and B. D. Appelbe, Phys. Rev. Lett. **118**, 155001 (2017).
[7] P. T. Campbell, C. A. Walsh, B. K. Russell, J. P. Chittenden, A. Crilly, G. Fiksel, P. M. Nilson, A. G. R. Thomas, K. Krushelnick, and L. Willingale, Phys. Rev. Lett. **125**, 145001 (2020).
[8] L. Willingale, A. G. R. Thomas, P. M. Nilson, M. C. Kaluza, S. Bandyopadhyay, A. E. Dangor, R. G. Evans, P. Fernandes, M. G. Haines, C. Kamperidis *et al.*, Phys. Rev. Lett. **105**, 095001 (2010).
[9] J. A. Stamper, Laser Part. Beams **9**, 841 (1991).
[10] D. A. Tidman and R. A. Shanny, Phys. Fluids **17**, 1207 (1974).
[11] M. Sherlock and J. J. Bissell, Phys. Rev. Lett. **124**, 055001 (2020).
[12] A. S. Joglekar, A. G. R. Thomas, W. Fox, and A. Bhattacharjee, Phys. Rev. Lett. **112**, 105004 (2014).
[13] A. S. Liao, S. Li, H. Li, K. Flippo, D. Barnak, K. V. Kelso, C. Fiedler Kawaguchi, A. Rasmus, S. Klein, J. Levesque *et al.*, Phys. Plasmas **26**, 032306 (2019).
[14] P. Tzeferacos, A. Rigby, A. F. A. Bott, A. R. Bell, R. Bingham, A. Casner, F. Cattaneo, E. M. Churazov, J. Emig, F. Fiuza *et al.*, Nat. Commun. **9**, 591 (2018).
[15] E. M. Epperlein and M. G. Haines, Phys. Fluids **29**, 1029 (1986).
[16] W. A. Farmer, J. M. Koning, D. J. Strozzi, D. E. Hinkel, L. F. Berzak Hopkins, O. S. Jones, and M. D. Rosen, Phys. Plasmas **24**, 052703 (2017).
[17] J. R. Davies, D. H. Barnak, R. Betti, E. M. Campbell, P.-Y. Chang, A. B. Sefkow, K. J. Peterson, D. B. Sinars, and M. R. Weis, Phys. Plasmas **24**, 062701 (2017).
[18] J. J. Bissell, C. P. Ridgers, and R. J. Kingham, Phys. Rev. Lett. **105**, 175001 (2010).
[19] C. A. Walsh, J. P. Chittenden, D. W. Hill, and C. Ridgers, Phys. Plasmas **27**, 022103 (2020).
[20] M. G. Haines, Phys. Rev. Lett. **78**, 254 (1997).
[21] J. D. Sadler, H. Li, and B. M. Haines, Phys. Plasmas **27**, 072707 (2020).
[22] A. Nishiguchi, T. Yabe, and M. G. Haines, Phys. Fluids **28**, 3683 (1985).
[23] M. G. Haines, Plasma Phys. Controlled Fusion **28**, 1705 (1986).
[24] J. R. Davies, R. Betti, P.-Y. Chang, and G. Fiksel, Phys. Plasmas **22**, 112703 (2015).
[25] C. A. Walsh, K. McGlinchey, J. K. Tong, B. D. Appelbe, A. Crilly, M. F. Zhang, and J. P. Chittenden, Phys. Plasmas **26**, 022701 (2019).
[26] C. A. Walsh, A. J. Crilly, and J. P. Chittenden, Nucl. Fusion **60**, 106006 (2020).
[27] J.-Y. Ji and E. D. Held, Phys. Plasmas **20**, 042114 (2013).
[28] A. Bendib, D. Bennaceur-Doumaz, and F. El Lemdani, Phys. Plasmas **9**, 1555 (2002).

[29] I. Kotelnikov, Plasma Phys. Rep. **38**, 608 (2012).
[30] A. G. R. Thomas, M. Tzoufras, A. P. L. Robinson, R. J. Kingham, C. P. Ridgers, M. Sherlock, and A. R. Bell, J. Comput. Phys. **231**, 1051 (2012).
[31] M. Tzoufras, A. R. Bell, P. A. Norreys, and F. S. Tsung, J. Comput. Phys. **230**, 6475 (2011).
[32] J. F. Luciani, P. Mora, and J. Virmont, Phys. Rev. Lett. **51**, 1664 (1983).
[33] J. P. Brodrick, M. Sherlock, W. A. Farmer, A. S. Joglekar, R. Barrois, J. Wengraf, J. J. Bissell, R. J. Kingham, D. Del Sorbo, M. P. Read *et al.*, Plasma Phys. Controlled Fusion **60**, 084009 (2018).
[34] R. J. Henchen, M. Sherlock, W. Rozmus, J. Katz, D. Cao, J. P. Palastro, and D. H. Froula, Phys. Rev. Lett. **121**, 125001 (2018).
[35] See Supplemental Material at http://link.aps.org/supplemental/10.1103/PhysRevLett.126.075001 for transport coefficient fit functions.
[36] D. W. Hill and R. J. Kingham, Phys. Rev. E **98**, 021201(R) (2018).
[37] K. M. Schoeffler and L. O. Silva, Phys. Rev. Research **2**, 033233 (2020).
[38] J. R. Davies, H. Wen, J-Y. Ji, and E. D. Held, Phys. Plasmas **28**, 012305 (2021).